nature geoscience

Article

https://doi.org/10.1038/s41561-024-01384-7

Emergent temperature sensitivity of soil organic carbon driven by mineral associations

In the format provided by the authors and unedited

Supplementary Materials for

Emergent temperature sensitivity of soil organic carbon driven by mineral associations

Katerina Georgiou, Charles D. Koven, William R. Wieder, Melannie D. Hartman, William J. Riley, Jennifer Pett-Ridge, Nicholas J. Bouskill, Rose Z. Abramoff, Eric Slessarev, Anders Ahlström, William J. Parton, Adam F. A. Pellegrini, Derek Pierson, Benjamin N. Sulman, Qing Zhu, Robert B. Jackson

Correspondence to: georgiou1@llnl.gov

This file includes:

Supplementary Figures 1 to 15 ……. 2
Supplementary Tables 1 to 6 …… 17
Supplementary References ……..…….. 23

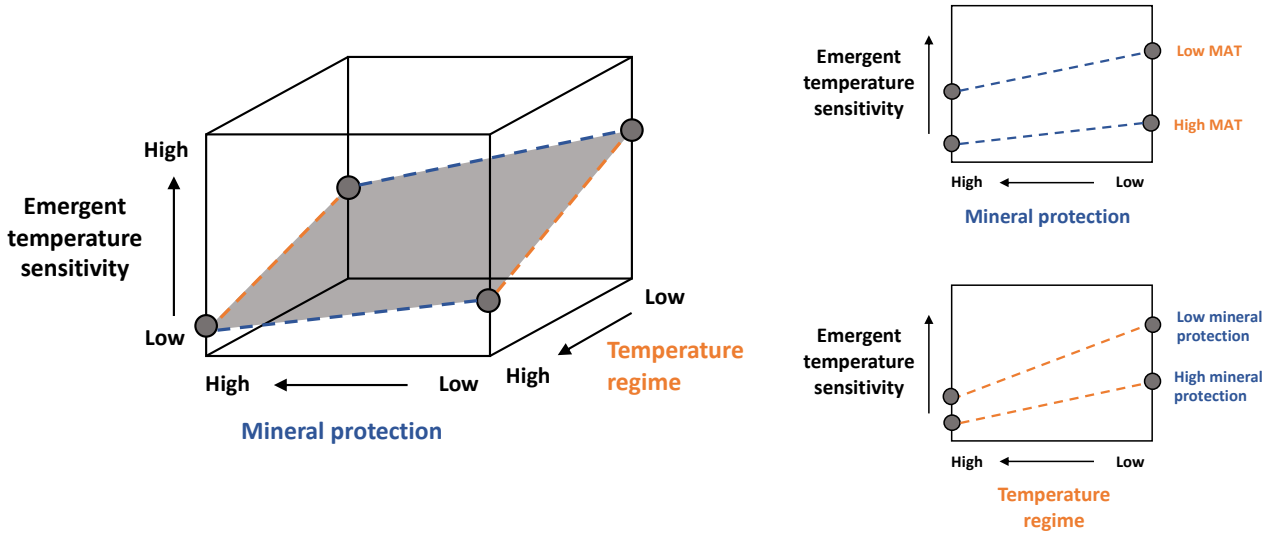

Supplementary Figure 1 | Conceptual schematic of the factors driving the emergent climatological temperature sensitivity of soil organic carbon. To illustrate the role of mineral-organic associations and ambient temperature on the emergent temperature sensitivity of bulk soil organic carbon, we expand on the framework of Davidson & Janssens[1]. The degree of mineral protection can affect the emergent temperature sensitivity of soil organic carbon, due to the distinct temperature sensitivities of underlying particulate and mineral-associated carbon pools. These differences in pool-specific temperature sensitivities can stem from limitations on the bioavailability of mineral-associated organic matter. Furthermore, the current temperature regime can also play a role in the intrinsic temperature sensitivity, where warm-adapted microbes may be relatively less sensitive to additional temperature increases.

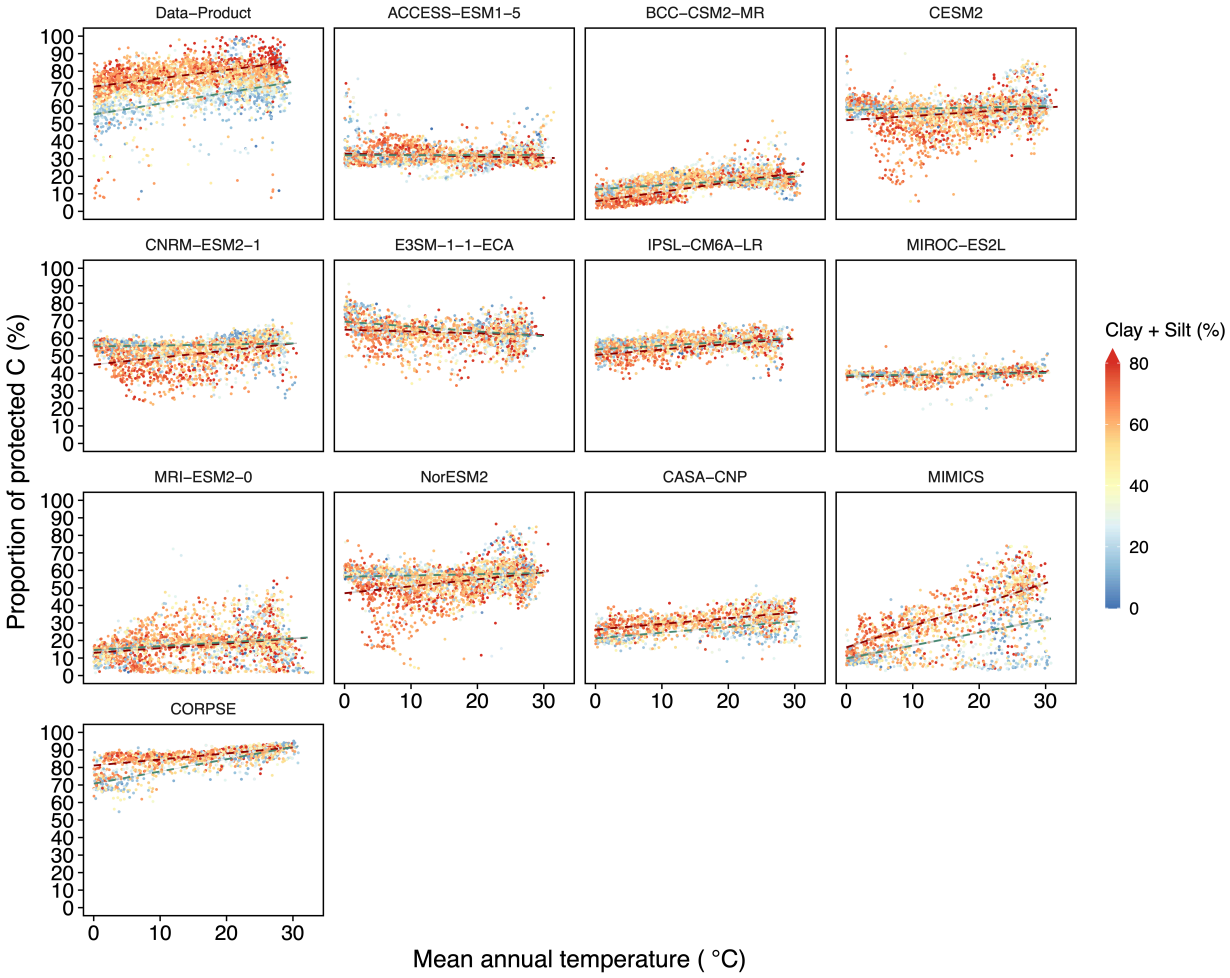

Supplementary Figure 2 | Proportion of total soil carbon that is protected as a function of climatological temperature and clay and silt minerals. Percentage of total soil carbon that is protected (i.e., mineral-associated) as a function of climatological temperature across non-permafrost mineral soils with mean annual temperatures above 0°C. Each gridcell is colored by the amount of clay and silt minerals. Best-fit trends are depicted for fine- and coarse-textured soils as red and blue dashed lines, respectively – here, fine-textured soils were classified as those with > 70% clay plus silt content and coarse-textured soils as < 20% clay plus silt content.

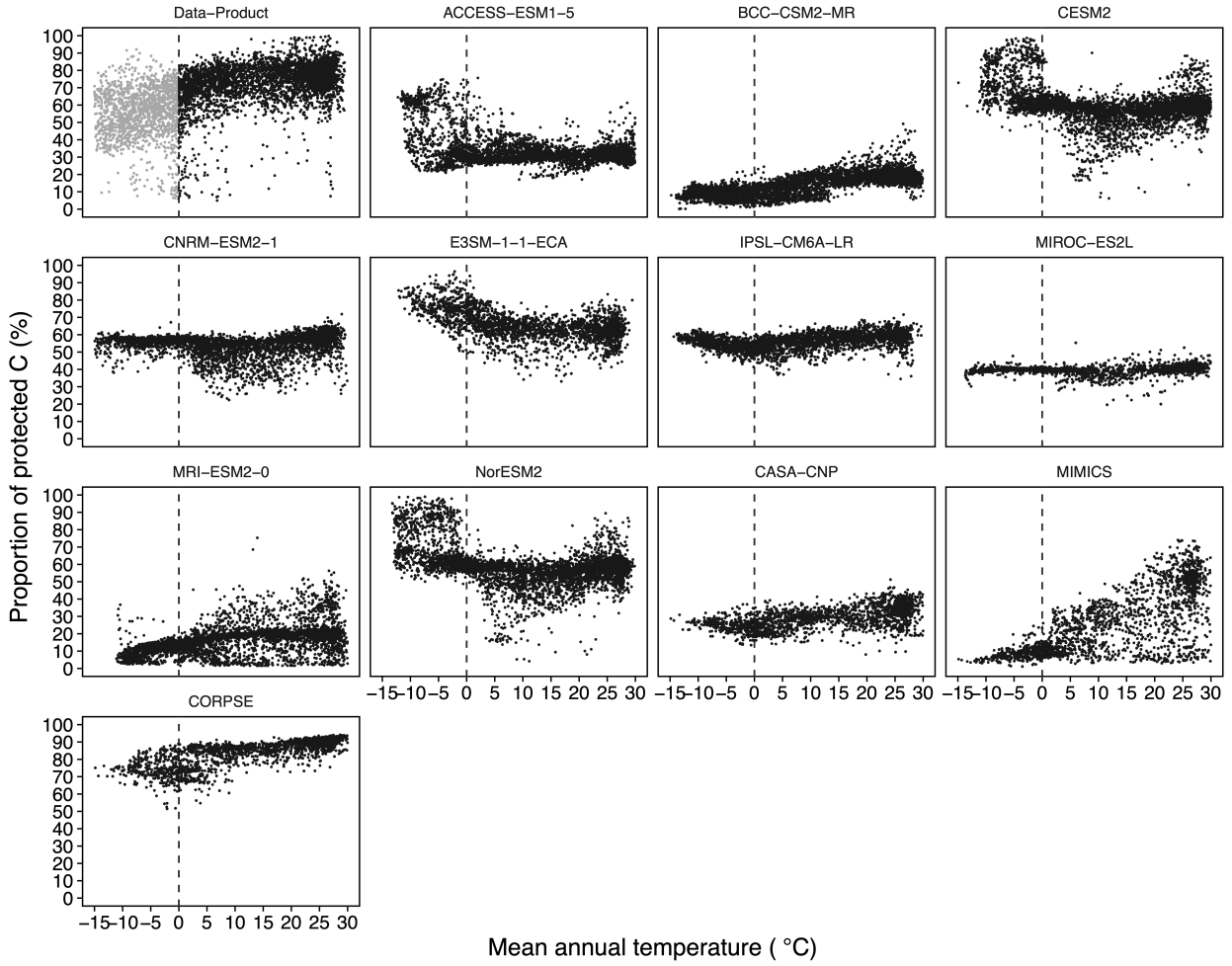

Supplementary Figure 3 | Proportion of total soil carbon that is protected as a function of climatological temperature across the data and models. Percentage of total soil carbon that is protected (i.e., mineral-associated) as a function of mean annual air temperature across all mineral soils globally. Each point depicts a gridcell. Dashed black lines are shown at 0°C. The data product is shaded below 0°C to denote that observations (in the synthesis used to derive the data product[2]) were limited in this climate regime and that further high-latitude measurements are needed in future studies (see Methods section '*Data sources and processing*'). Only gridcells with MAT > 0°C were included in subsequent analyses of climatological temperature sensitivities.

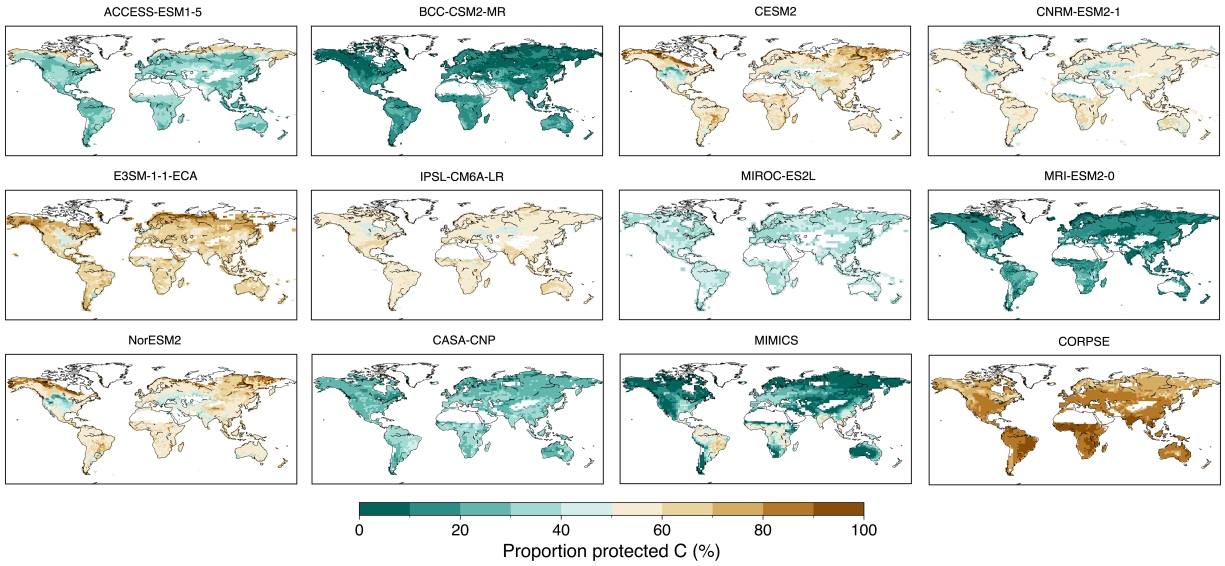

Supplementary Figure 4 | Proportion of soil carbon in protected pools globally. The percentage of total soil carbon that is protected across an ensemble of CMIP6 ESMs and offline land models. CMIP6 ESMs are detailed in Supplementary Table 1. Offline land models from the Biogeochemical Testbed are detailed in Supplementary Table 2.

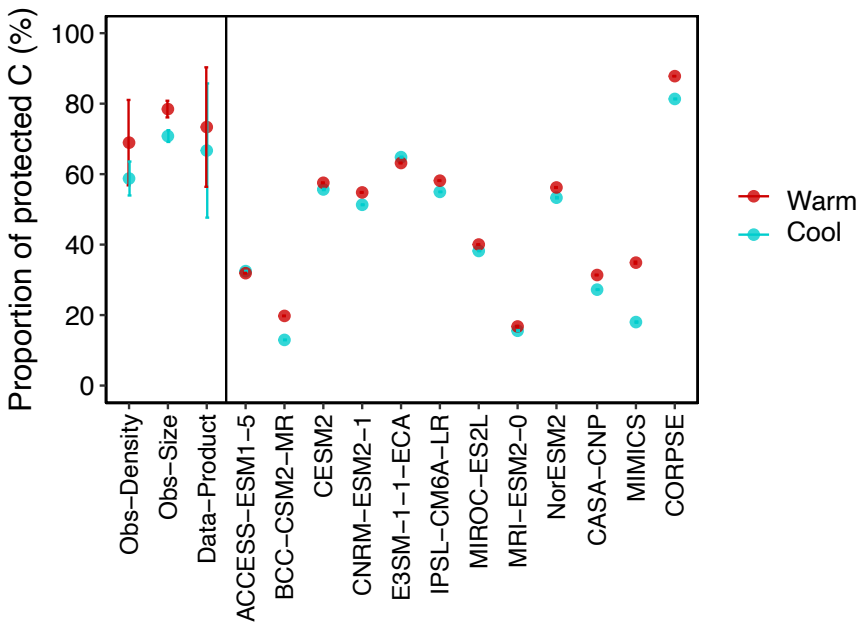

Supplementary Figure 5 | Proportion of soil carbon in protected pools across the data and models. The percentage of total soil carbon that is mineral-associated in the globally-gridded data product (n = 32,528 grid cells), the observational synthesis used to derive the data product[2] (summarized by density and size fractionation methods, with n = 203 and 1243, respectively), and across an ensemble of CMIP6 ESMs and offline land models (n = 32,528 grid cells). Estimates (global means and 90% confidence intervals on the mean) are given for non-permafrost mineral soils with mean annual temperatures above 0°C, separated within cool (< 15°C) and warm (≥ 15°C) climates. Data product uncertainty ranges correspond to 90% prediction intervals[2]. Values are summarized in Supplementary Table 5.

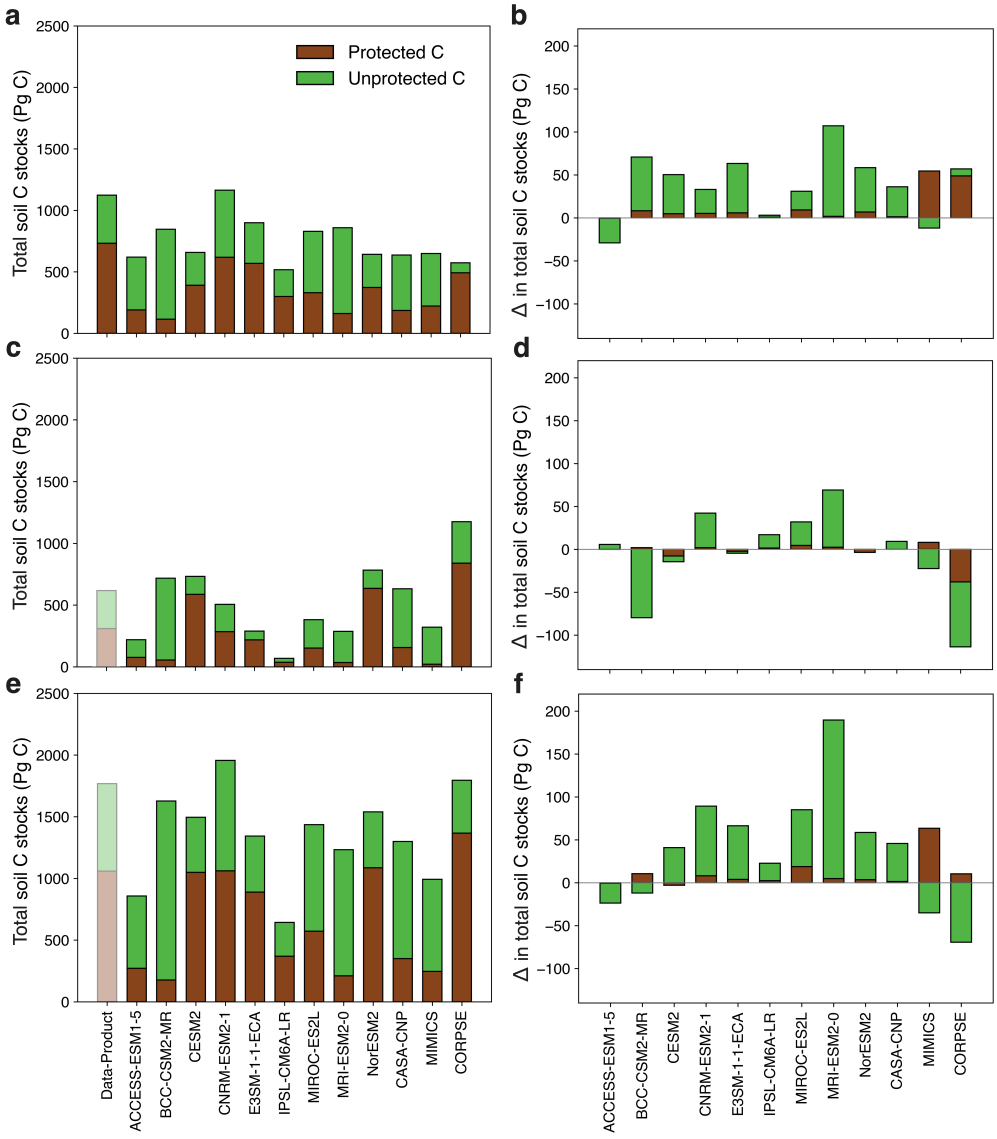

Supplementary Figure 6 | Global protected and unprotected soil C stocks across the data and models. a-f, Given estimates are for mineral soils with mean annual temperatures above 0°C **(a,b)** and below 0°C **(c,d)**, and globally for all temperatures **(e,f)**. The data product is shaded opaque below 0°C to depict that the observations (in the synthesis used to derive the data product[2]) were limited in this climate regime and that further high-latitude measurements are needed in future studies (see Methods section '*Data sources and processing*'). **a,c,e,** Distribution of present day protected and unprotected C stocks across the data and models. Values are summarized in Supplementary Table 4, including 90% prediction intervals from the data product. **b,d,f,** Changes in protected and unprotected soil C stocks under SSP5-8.5 for the CMIP6 ESMs and RCP8.5 for the offline land models at the end of the 21st century (2090-2100) compared to present day (2005-2015). CMIP6 ESMs and offline land models (CASA-CNP, MIMICS, and CORPSE) are detailed in Supplementary Tables 1 and 2, respectively. MIMICS and CORPSE constitute the two microbial-explicit soil carbon models used in this study.

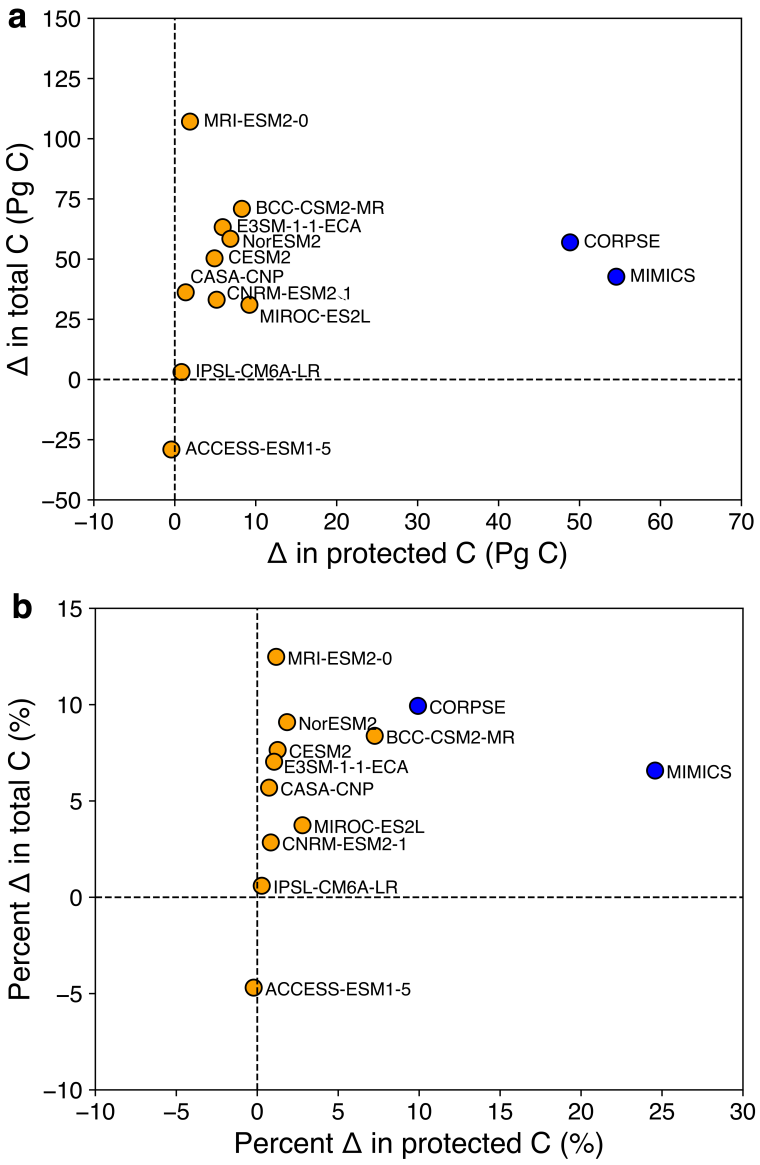

Supplementary Figure 7 | Change in total and protected soil carbon stocks in 2100. a-b, Absolute **(a)** and relative percent **(b)** change in total and protected soil carbon stocks under SSP5-8.5 for the CMIP6 ESMs and RCP8.5 for the offline land models at the end of the 21st century (2090-2100) compared to present day (2005-2015). Given estimates are for non-permafrost mineral soils with mean annual temperatures above 0°C. CMIP6 ESMs and offline land models (CASA-CNP, MIMICS, and CORPSE) are detailed in Supplementary Tables 1 and 2, respectively. MIMICS and CORPSE (shown in blue) constitute the two microbial-explicit soil carbon models used in this study.

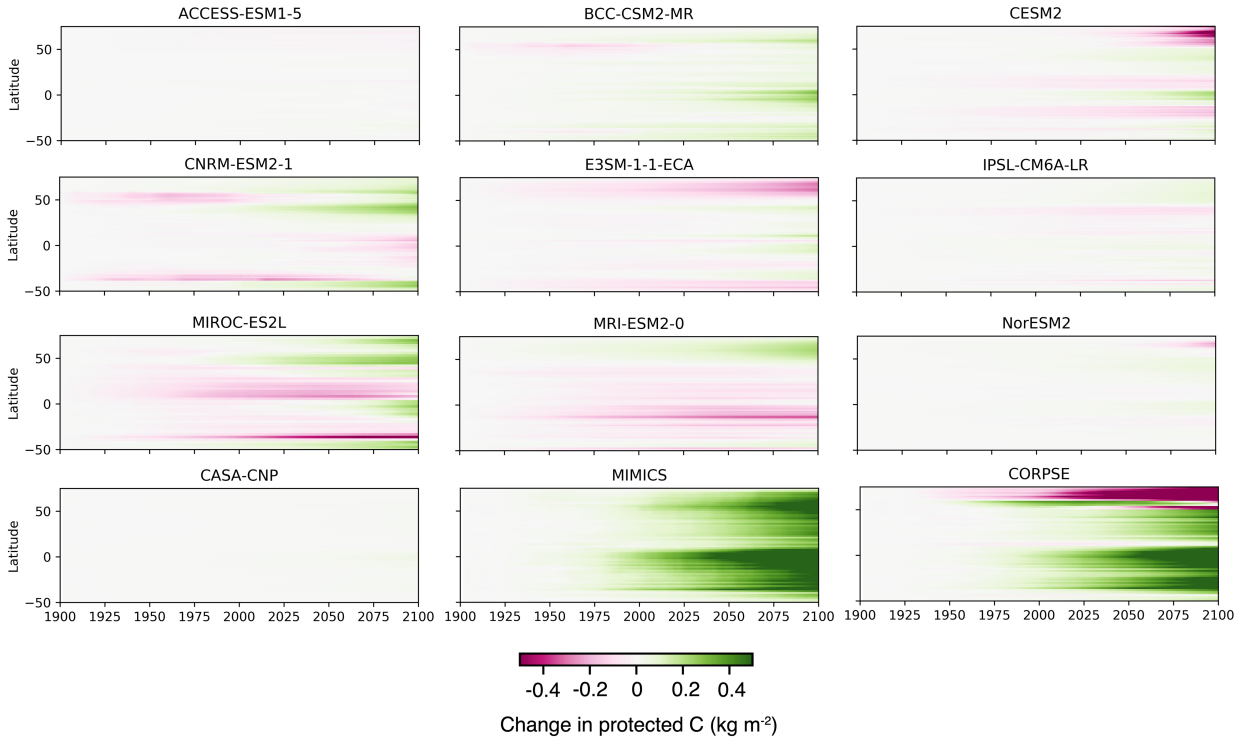

Supplementary Figure 8 | Projections of protected soil carbon stocks across CMIP6 ESMs and offline land models. Model projections depict historical runs to present day and SSP5-8.5 for the CMIP6 ESMs and RCP8.5 for the offline land models, each compared to historical stocks (1900-1910). CMIP6 ESMs and offline land models (CASA-CNP, MIMICS, and CORPSE) are detailed in Supplementary Tables 1 and 2, respectively. MIMICS and CORPSE constitute the two microbial-explicit soil carbon models used in this study.

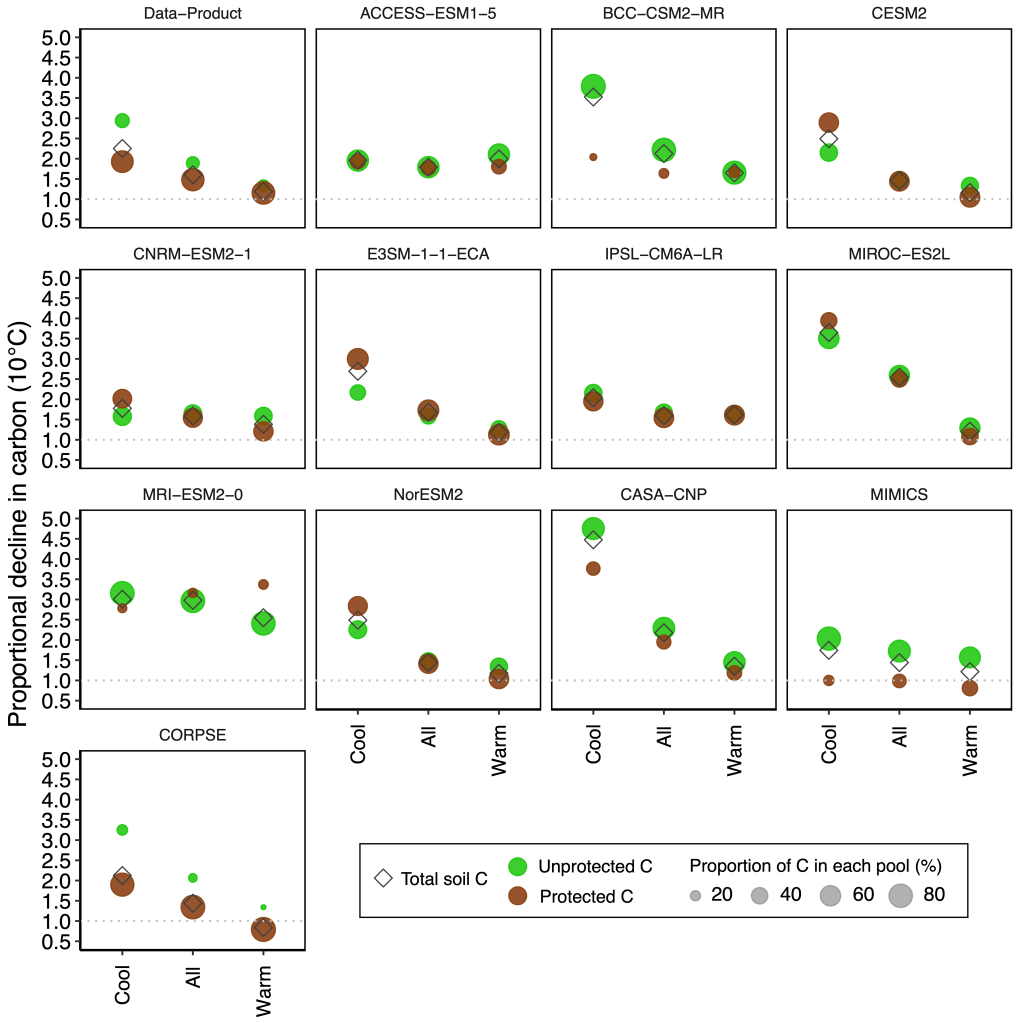

Supplementary Figure 9 | Climatological temperature sensitivity of total soil carbon and the contribution of underlying protected and unprotected pools across global data and models. The climatological temperature sensitivity of total soil carbon (denoted by a diamond) is an emergent property of the temperature sensitivity of protected (i.e., mineral-associated; brown circles) and unprotected (i.e., particulate; green circles) soil carbon pools, as well as the proportion of carbon within each of these underlying pools (denoted by the marker area). The proportional decline in carbon for a 10°C increase in mean annual temperature was calculated for each carbon pool and in each climate regime, controlling for potential confounding variables (see Methods). Following previous studies[3], and balancing the number of data points in each climate regime in the globally-gridded data, the cool-warm threshold was aligned approximately with the mean value of the annual temperatures across all gridcells with temperatures above freezing and excluding soils limited by saturation or aridity; i.e., cool (< 15°C) and warm (≥ 15°C) regions, and all temperatures (> 0°C). Results are shown for the data product, CMIP6 ESMs, and offline land models. 95% confidence intervals are given in Supplementary Table 6. Higher values (> 1) indicate greater decreases in carbon with increases climatological temperature, lower values (< 1) indicate increases in carbon, and values equal to 1 (grey dotted line) indicate thermal independence.

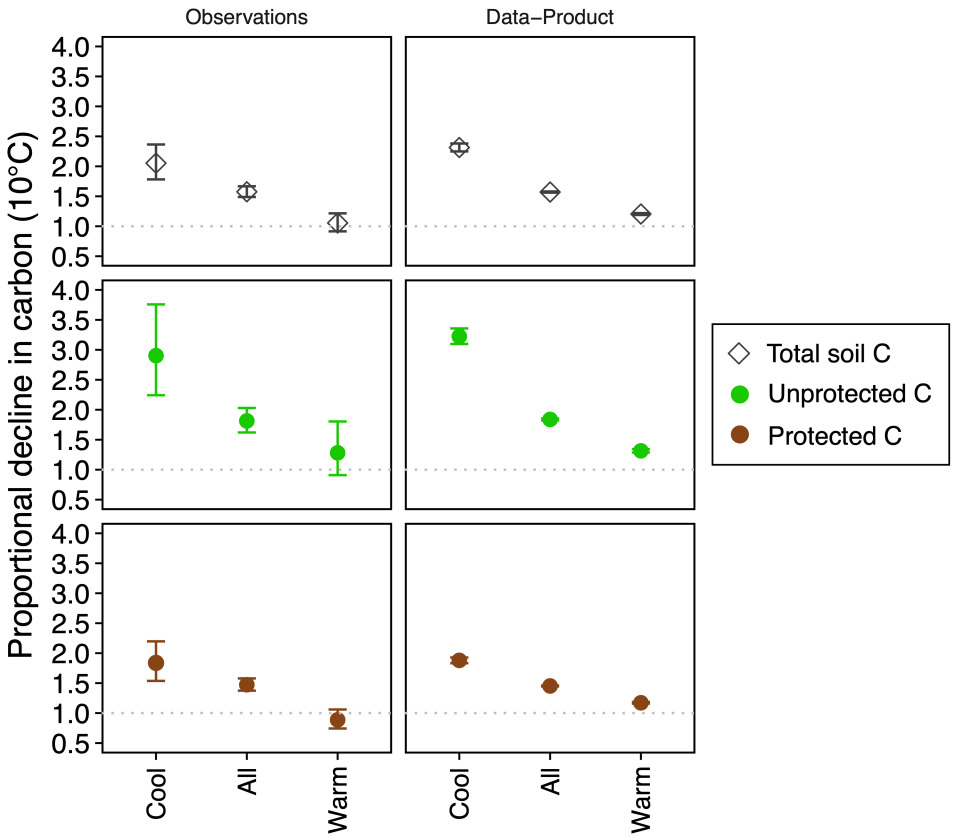

Supplementary Figure 10 | Climatological temperature sensitivity of total soil carbon and underlying protected and unprotected pools in observations. Climatological temperature sensitivities of total (denoted by a diamond), protected (i.e., mineral-associated; brown circles), and unprotected (i.e., particulate; green circles) soil carbon in the globally-gridded data product and the observational synthesis (i.e., the observations used to derive the data product[2]). The temperature sensitivities were calculated as the proportional decline in carbon stocks for a 10°C increase in mean annual temperature, controlling for potential confounding variables (namely, precipitation and texture; see Methods). For the observations, three pedotransfer functions of bulk density (averaging from refs.[4,5], given performance results in ref.[6]) were used to convert carbon concentrations to stocks. We note that the observations were limited in warmer climates[2], and we strongly encourage additional measurements in these regions. To better balance the number of observations in each climate regime, the cool-warm threshold was aligned with the mean value of the annual temperatures across the observations; i.e., cool (< 12°C) and warm (≥ 12°C) regions, and all temperatures (> 0°C). The analogous calculations are presented for the data product across each temperature regime (and using a random subsampling in Supplementary Fig. 11). Error bars denote 95% confidence intervals. The general agreement between the observations and data product provides further evidence for the robustness of the reported temperature sensitivity trends between protected and unprotected carbon (Fig. 2c). Higher values (> 1) indicate greater decreases in carbon with increases climatological temperature, lower values (< 1) indicate increases in carbon, and values equal to 1 (dotted line) indicate thermal independence.

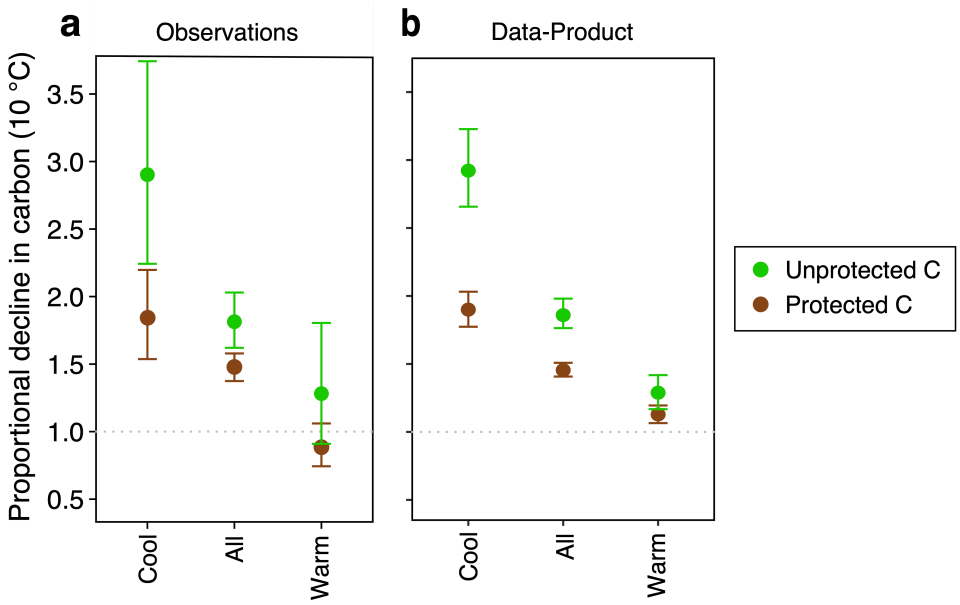

Supplementary Figure 11 | Climatological temperature sensitivity of protected and unprotected soil carbon pools in observations. Climatological temperature sensitivities of protected (i.e., mineral-associated; brown circles) and unprotected (i.e., particulate; green circles) soil carbon in the observations and globally-gridded data product[2], calculated as the proportional decline in carbon stocks for a 10°C increase in mean annual temperature, controlling for potential confounding variables (namely, precipitation and texture; see Methods). **a,** For the observations (n = 1446), climatological temperature sensitivities of protected and unprotected carbon were summarized from the corresponding panels in Supplementary Fig. 10. **b,** We randomly subsampled the data product to have approximately the same number of data points as the raw observations (conservatively, n = 1000). We then calculated the corresponding temperature sensitivity of each pool, and iterated this subsampling 500 times to build a distribution of temperature sensitivities, from which we calculated the mean (green and brown circles) and 95% confidence intervals (error bars) shown. Data products often exhibit less overall noise compared to their respective raw observations (e.g., in refs. [7–9]). Unsurprisingly, random subsampling of the data product to have approximately the same number of data points as the raw observations increased the confidence intervals (e.g., compared to Supplementary Fig. 10), but importantly did not affect the statistical differences between pools and their trends across climates (Fig. 2c). Higher values (> 1) indicate greater decreases in carbon with increases climatological temperature, lower values (< 1) indicate increases in carbon, and values equal to 1 (dotted line) indicate thermal independence.

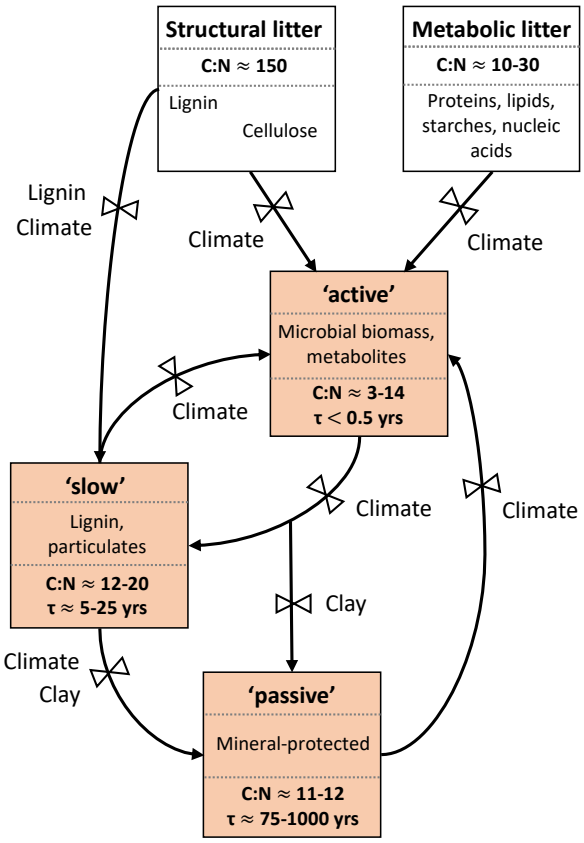

Supplementary Figure 12 | Conceptual schematic of the first-order soil C models analyzed in this study. Interpretability of pools and flows in the Century and CASA-CNP models, and their derivatives in CMIP6 ESMs. Redrawn from Parton et al.[17,18] (see Methods section '*Model pool interpretability*').

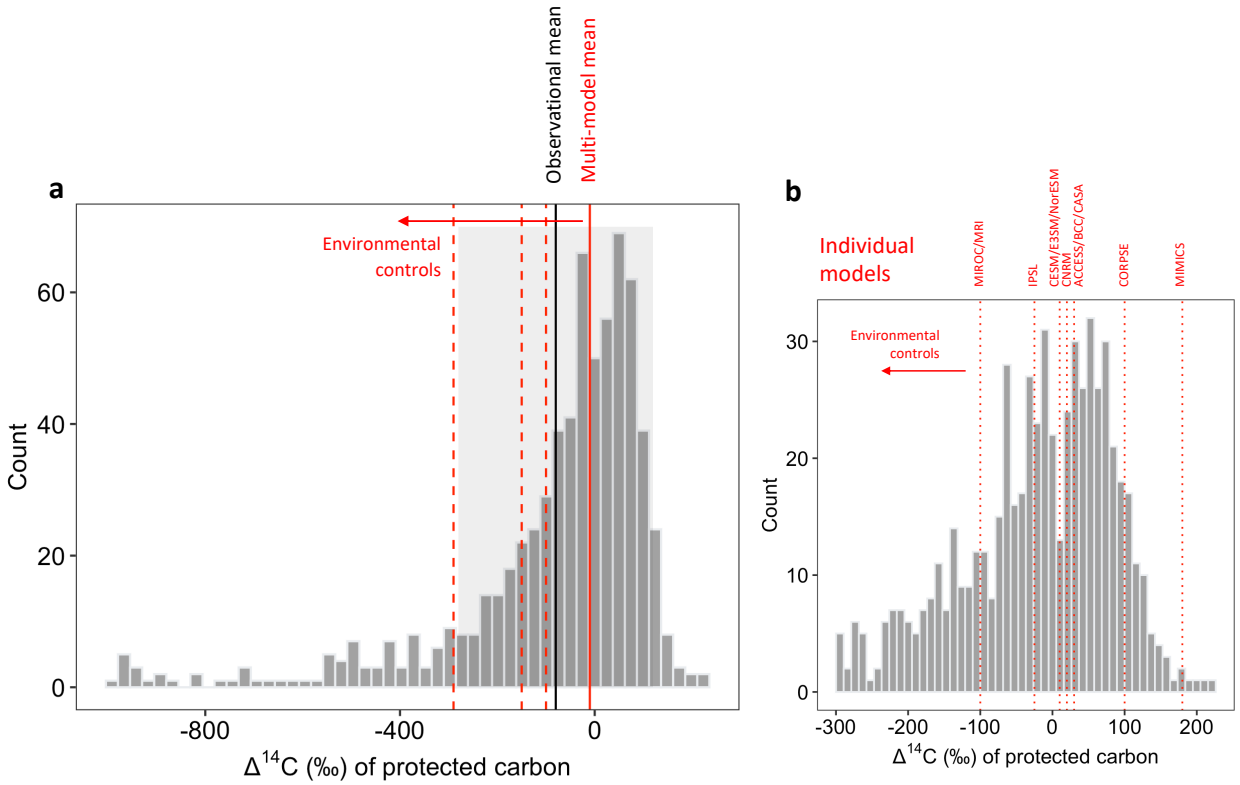

Supplementary Figure 13 | Radiocarbon measurements and intrinsic model turnover times of protected carbon. Histogram of measured $\Delta^{14}C$ (‰) from the 'protected' (i.e., mineral-associated) carbon fraction in the International Soil Radiocarbon Database[10–12] (ISRaD; n = 682 observations). **a,** The observational mean value is depicted with a solid black line and one standard deviation is shown with grey shading. Mean carbon ages are summarized in Supplementary Table 3, following Shi et al.[13] to convert between $\Delta^{14}C$ and carbon ages as a cursory comparison to model pool turnover times. We note that the measurements span soil profiles globally, whereas for the models, intrinsic turnover times are reported in Supplementary Table 3 without environmental modifiers. We depict the multi-model mean in red, where the solid red line shows the intrinsic (baseline) turnover time and the red dashed lines show approximate turnover times accounting for environmental controls (namely, temperature and moisture) in temperate forest, tall grass prairie, and arctic tundra (following the red arrow from right to left, respectively) using environmental modifiers from the Century model[14]. Future work could estimate the distribution of $\Delta^{14}C$ values for each modeled soil carbon pool, by explicitly modeling a radiocarbon tracer and accounting for environmental controls in each gridcell. **b,** Subset of **(a)** where dotted red lines depict the intrinsic (baseline) turnover time of the protected carbon pool in each of the global models, and the red arrow represents the directionality of environmental modifiers.

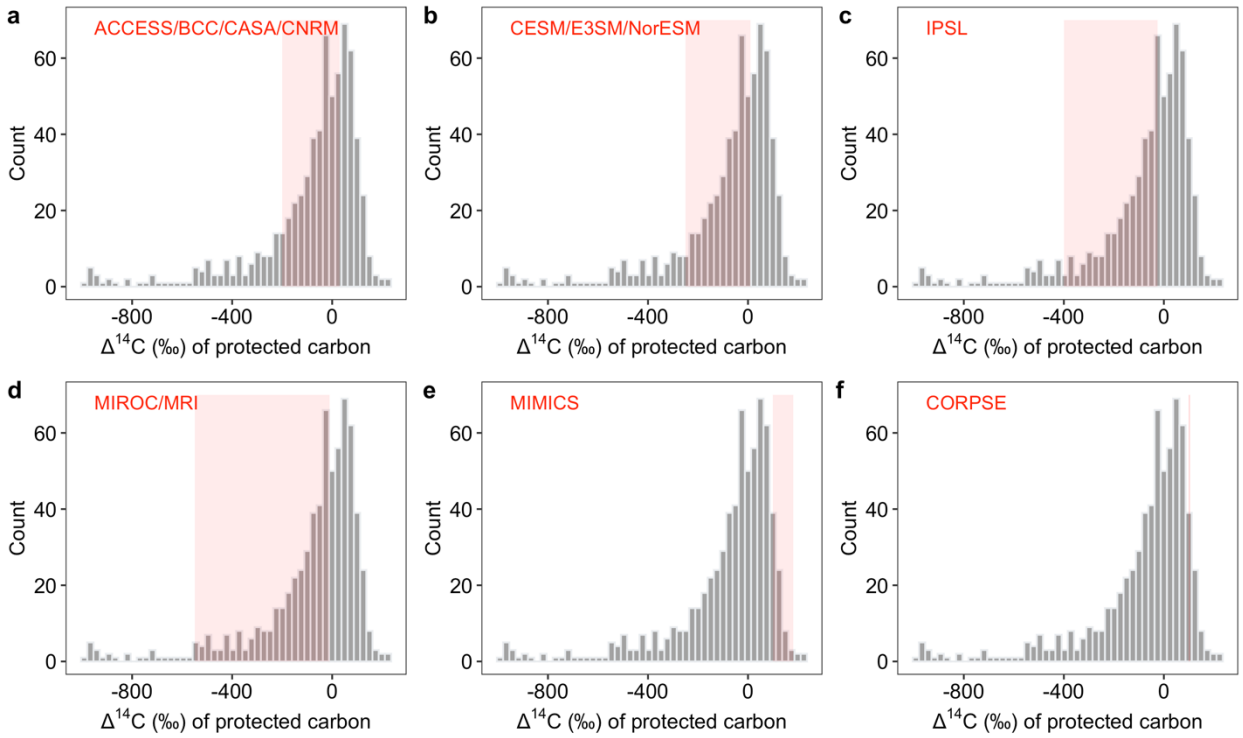

Supplementary Figure 14 | Radiocarbon measurements and approximate model turnover times of protected carbon, accounting for environmental controls. a-f, Histogram of measured $\Delta^{14}C$ (‰) from the 'protected' (i.e., mineral-associated) carbon fraction in the International Soil Radiocarbon Database[10–12] (ISRaD; n = 682 observations). Protected C turnover time (τ) ranges for each global model are shaded in red. The ranges depict approximate rate modifiers for environmental conditions. Namely, for the CMIP6 ESMs, we estimate and apply an environmental modifier (based on temperature and moisture) on the decomposition rate, using the parameterization of the Century model[14] – i.e., up to a factor of ~10 decrease in decomposition rate (increase in τ) in arctic regions compared to the intrinsic (baseline) values. In contrast, the τ range for MIMICS results from a dependence on soil texture only, and CORPSE uses a fixed turnover time for protected carbon[15]. $\Delta^{14}C$ values are approximated from the model turnover times (following Shi et al. [13]) as a cursory comparison to measurements. Future work could estimate the distribution of $\Delta^{14}C$ values for each modeled soil carbon pool, by explicitly modeling a radiocarbon tracer and accounting for environmental controls in each gridcell.

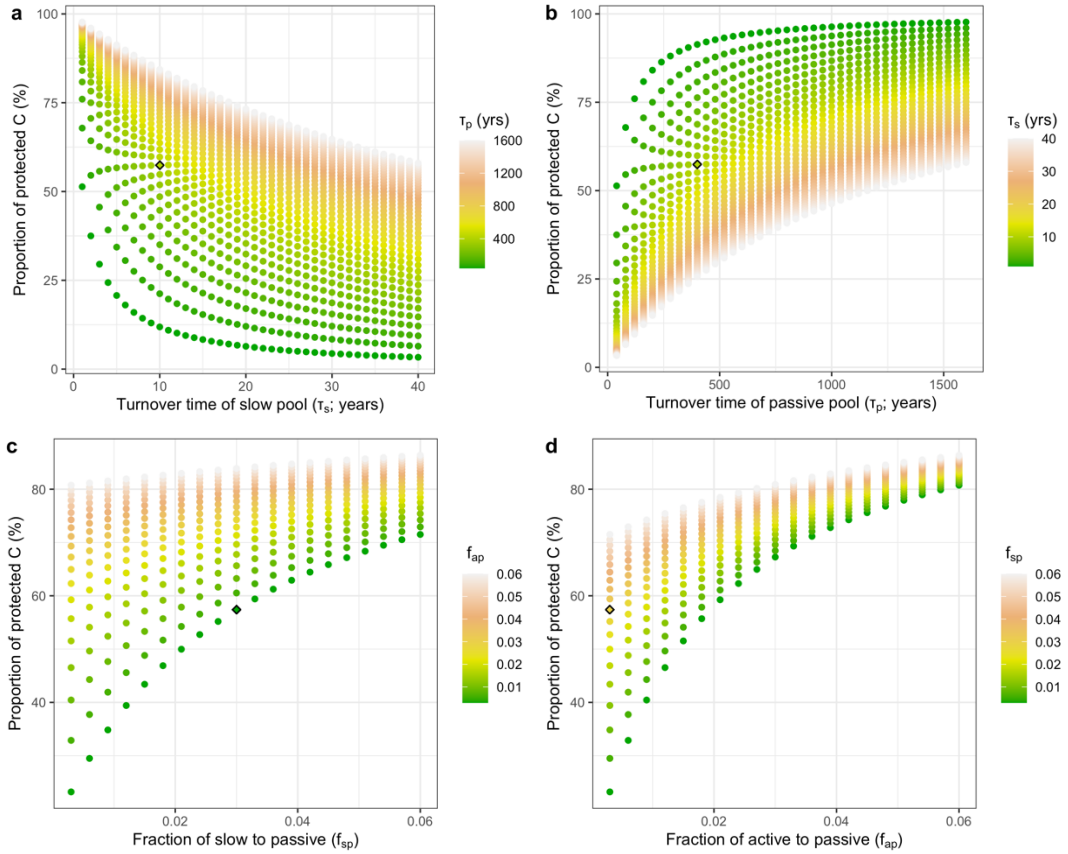

$$\frac{d}{dt}\begin{bmatrix} C_a \\ C_s \\ C_p \end{bmatrix} = \begin{bmatrix} f_a \\ 1-f_a \\ 0 \end{bmatrix} \cdot I + \begin{bmatrix} -k_a & (1-f_{sp}-f_{sCO2})\cdot k_s & f_{pa}\cdot k_p \\ (1-f_{ap}-f_{aCO2})\cdot k_a & -k_s & f_{ps}\cdot k_p \\ f_{ap}\cdot k_a & f_{sp}\cdot k_s & -k_p \end{bmatrix} \begin{bmatrix} C_a \\ C_s \\ C_p \end{bmatrix}$$

$$\begin{bmatrix} C_a \\ C_s \\ C_p \end{bmatrix}_{SS} = \begin{bmatrix} -k_a & (1-f_{sp}-f_{sCO2})\cdot k_s & f_{pa}\cdot k_p \\ (1-f_{ap}-f_{aCO2})\cdot k_a & -k_s & f_{ps}\cdot k_p \\ f_{ap}\cdot k_a & f_{sp}\cdot k_s & -k_p \end{bmatrix}^{-1} \begin{bmatrix} f_a \\ 1-f_a \\ 0 \end{bmatrix} \cdot (-I)$$

Supplementary Figure 15 | Parameter sensitivity analysis for the proportion of protected soil carbon in a three-pool, first-order model. a-d, The slowest-cycling ('passive') carbon pool (C_p) was used to represent mineral-protected carbon, whereas the intermediate-cycling ('slow') pool (C_s) most closely corresponds to particulate carbon (see Methods section on '*Model pool interpretability*'). Here we used parameters from IPSL-CM6A-LR (IPSL source code[16]) – namely, $k_a = \frac{1}{0.14} yr^{-1}, k_s = \frac{1}{10} yr^{-1}, k_p = \frac{1}{444} yr^{-1}, f_a = 0.6, f_{ap} = 0.003, f_{aCO2} = 0.85, f_{sp} = 0.03, f_{sCO2} = 0.55, f_{pa} = 0.45, f_{ps} = 0$ with the original steady-state shown as a black diamond. We calculated the sensitivity in steady-state pool distributions with a range of parameter combinations: **a,** $\tau_s = \frac{1}{k_s}$, **b,** $\tau_p = \frac{1}{k_p}$, **c,** f_{sp}, **d,** f_{ap}. We note that the exact parameters used in this exercise are not important, but rather we aim to illustrate broad patterns in the proportion of protected ('passive') carbon; for instance, one modification could be to increase the fraction of active carbon that flows to passive (i.e., f_{ap}) and/or increase the dependence of this parameter on soil texture. Currently the flows appear to be aligned with a conceptualization of mineral protection, but the parameterization could be further refined. In future work, soil C pool ages could be used as additional constraints (Supplementary Fig. 13).

Supplementary Table 1 | CMIP6 Earth system models analyzed in this study.

Earth system model	Land sub-model	Institute	References
ACCESS-ESM1-5	CABLE2.4	Commonwealth Scientific and Industrial Research Organization (Australia)	Ziehn et al. (2020)[19]
BCC-CSM2-MR	BCC-AVIM2	Beijing Climate Center (China)	Wu et al (2019)[20]
CESM2	CLM5	National Center for Atmospheric Research (USA)	Danabasoglu et al. (2020)[21]
CNRM-ESM2-1	ISBA-CTRIP	Centre National de Recherches Météorologiques (France)	Séférian et al. (2020)[22]
E3SM-1-1-ECA	ELM-ECA	Department of Energy (USA)	Burrows et al. (2020)[23]
IPSL-CM6A-LR	ORCHIDEE	Institut Pierre Simon Laplace (France)	Boucher et al. (2020)[24]
MIROC-ES2L	VISIT-e	Japan Agency for Marine-Earth Science and Technology (Japan)	Hajima et al. (2020)[25]
MRI-ESM2-0	HAL	Meteorological Research Institute (Japan)	Yukimoto et al. (2019)[26]
NorESM2-LM	CLM5	Center for International Climate and Environmental Research (Norway)	Seland et al. (2020)[27]

Supplementary Table 2 | Offline soil carbon models analyzed in this study.

Offline soil model	Land forcing	Features	References
CASA-CNP	CLM	3 soil carbon pools (excl. litter); first-order kinetics; implicit microbial and mineral-associated processes	Wieder et al. (2019)[15]; Potter et al. (1993)[28]
MIMICS	CLM	5 soil carbon pools (excl. litter, incl. microbial biomass); explicit microbial and mineral-associated processes; only microbially inputs into mineral-protected	Wieder et al. (2019)[15]; Wieder et al. (2015)[29]
CORPSE	CLM	7 soil carbon pools (excl. litter, incl. microbial biomass); explicit microbial and mineral-associated processes; plant & microbial inputs into mineral-protected	Wieder et al. (2019)[15]; Sulman et al. (2014)[30]

Supplementary Table 3 | Details regarding protected carbon in the CMIP6 ESMs and offline land models.

Earth system model	Land/soil sub-model	No. of soil pools (excl. litter)	No. of pools grouped into protected C	Kinetics of flows into/out of protected pool(s)	Clay + silt increase flow to protected carbon	Intrinsic turnover time (τ) of protected carbon[#]	References
ACCESS-ESM1-5	CABLE2.4/ CASA-CNP	3	1	First-order (linear)	Y[*]	τ ~ 222 years[*]	Ziehn et al. (2020)[19] Wang et al. (2010)[31] Randerson et al. (1997)[32]
BCC-CSM2-MR	BCC-AVIM2/ CESVA	3	1	First-order (linear)	Y	τ ~ 220 years	Cao & Woodward (1998)[33] Parton et al. (1988)[14]
CESM2	CLM5	3	1	First-order (linear)	Y	τ ~ 270 years	Lawrence et al. (2019)[34] Koven et al. (2013)[35] Parton et al. (1988)[14]
CNRM-ESM2-1	ISBA-CTRIP	3	1	First-order (linear)	Y	τ ~ 240 years	Séférian et al. (2020)[22] Parton et al. (1988)[14]
E3SM-1-1-ECA	ELM-ECA	3	1	First-order (linear)	Y	τ ~ 270 years	Lawrence et al. (2019)[34] Koven et al. (2013)[35] Parton et al. (1988)[14]
IPSL-CM6A-LR	ORCHIDEE 3	3	1	First-order (linear)	Y	τ ~ 444 years	Boucher et al. (2020)[24] Krinner et al. (2005)[36] Parton et al. (1988)[14] IPSL source code[16]
MIROC-ES2L	VISIT-e	3	1	First-order (linear)	Y[*]	τ ~ 1000 years[*]	Hajima et al. (2020)[25] Ito and Oikawa (2002)[37] Parton et al. (1994)[18]
MRI-ESM2-0	HAL	2	1	First-order (linear)	Y	τ ~ 1000 years	Yukimoto et al. (2019)[26] He et al. (2016)[38]
NorESM2-LM	CLM5	3	1	First-order (linear)	Y	τ ~ 270 years	Lawrence et al. (2019)[34] Koven et al. (2013)[35] Parton et al. (1988)[14]
CASA-CNP		3	1	First-order (linear)	Y	τ ~ 222 years	Wieder et al. (2019)[15] Potter et al. (1993)[28] Wang et al. (2010)[31]
MIMICS		5	1	First-order (linear)	Y	τ ~ 15-80 years (texture-dependent)	Wieder et al. (2019)[15] Wieder et al. (2015)[29]
CORPSE		7	3	First-order (linear)	Y	τ ~ 75 years	Wieder et al. (2019)[15] Sulman et al. (2014)[30]
Multi-model mean						τ ~ 370 years (w/out environ. controls[#])	
Data						C age ~ 800 (70, 3000) years[**]	Heckman et al. (2022)[11] Heckman et al. (2021)[12]

[#] Turnover times (τ) correspond to 1/k, where k is the intrinsic (baseline) first-order decay rate of the protected carbon pool. This baseline value is the maximum k (minimum τ) for protected carbon in each model. Environmental modifiers further increase τ in most gridcells; e.g., by a factor of ~2.5 in temperate forest to ~4 in tall grass prairie in the Century model[14].

[*] Using parameter values from the original CASA-CNP or Century models, based on the references cited for ACCESS-ESM1-5 and MIROC-ES2L, respectively. All other ESMs directly provided parameter values in the references cited.

[**] Mean value (with one standard deviation in parentheses; n = 682) for mineral-associated carbon from the International Soil Radiocarbon Database (ISRaD); mean C ages are approximated from $\Delta^{14}C$ values of -80‰ (120, -280), respectively (see Supplementary Fig. 13). Note that the data span profiles globally, whereas for the models, intrinsic τ is given without environmental modifiers.

Supplementary Table 4 | Comparison of total and protected soil carbon stocks in present day (2005-2015) and under SSP5-8.5 for CMIP6 ESMs and RCP8.5 for offline models (2090-2100). Given estimates are for non-permafrost mineral soils with mean annual temperatures above 0°C. Data product uncertainty ranges in parentheses correspond to 90% prediction intervals[2]. Global stocks and changes are summarized for all temperature regimes in Supplementary Fig. 6.

Source	Total soil C (Pg C)		Protected soil C (Pg C)		Proportion protected C (%; global mean)	
	Current	Δ (RCP8.5)	Current	Δ (RCP8.5)	Current	Δ (RCP8.5)
ACCESS-ESM1-5	611	-27	187	0	32	+2
BCC-CSM2-MR	823	+74	112	+8	17	-2
CESM2	646	+50	383	+5	57	-3
CNRM-ESM2-1	1148	+35	610	+5	53	1
E3SM-1-1-ECA	888	+64	561	+6	64	-4
IPSL-CM6A-LR	513	+5	298	+1	57	-1
MIROC-ES2L	812	+32	324	+9	39	0
MRI-ESM2-0	846	+102	159	+2	16	-1
NorESM2-LM	633	+58	367	+7	55	-4
CASA-CNP	622	+35	182	+1	30	-1
MIMICS	640	+42	220	+53	28	+5
CORPSE	564	+56	485	+48	85	-1
Data Product	1053	—	745 (614, 927)	—	70 (58, 86)	—

Supplementary Table 5 | Proportion of soil carbon in protected pools globally across the data and models. The percentage of total soil carbon that is protected in the data product, observational synthesis (i.e., the observations used to derive the data product[2]) summarized by particle size and density fractionation methods, and across an ensemble of CMIP6 ESMs and offline land models. Data product uncertainty ranges correspond to 90% prediction intervals[2]. Global means (with 90% confidence intervals on the mean) are given for non-permafrost mineral soils with mean annual temperatures above 0°C, and further separated within cool (< 15°C) and warm (> 15°C) climates.

Source	Proportion protected C (%)		
	All (MAT > 0°C)	Cool (MAT < 15°C)	Warm (MAT > 15°C)
ACCESS-ESM1-5	32	32	32
BCC-CSM2-MR	17	13	20
CESM2	57	57	58
CNRM-ESM2-1	53	51	55
E3SM-1-1-ECA	64	65	63
IPSL-CM6A-LR	57	55	58
MIROC-ES2L	39	38	40
MRI-ESM2-0	16	16	17
NorESM2-LM	55	53	56
CASA-CNP	30	27	32
MIMICS	28	18	34
CORPSE	85	81	88
Model Mean	44 (31, 57)	42 (28, 55)	46 (33, 59)
Data Product	70 (58, 86)	66 (47, 85)	73 (56, 90)
Observations (particle size)	72 (71, 74)	70 (69, 72)	78 (76, 80)
Observations (density)	61 (56, 66)	59 (54, 64)	69 (57, 81)

Supplementary Table 6 | Climatological temperature sensitivity of total, protected, and unprotected soil carbon stocks across temperature regimes. Proportional decline of each soil carbon pool with an increase in temperature of 10°C (denoted in 'value' columns) across each mean annual temperature (MAT) regime. Each climatological temperature sensitivity was calculated from the slope of the temperature relationship in each multiple linear regression model (see Methods), with corresponding 95% confidence intervals in parentheses (denoted in 'low' and 'high' columns).

	Total soil C			Protected soil C			Unprotected soil C			Temperature
	Value	Low	High	Value	Low	High	Value	Low	High	Regime
Data-Product	1.60	(1.59 ,	1.61)	1.48	(1.47 ,	1.49)	1.89	(1.88 ,	1.91)	MAT > 0°C
ACCESS-ESM1-5	1.79	(1.78 ,	1.80)	1.78	(1.77 ,	1.78)	1.79	(1.78 ,	1.80)	MAT > 0°C
BCC-CSM2-MR	2.13	(2.11 ,	2.14)	1.64	(1.62 ,	1.65)	2.22	(2.20 ,	2.24)	MAT > 0°C
CESM2	1.46	(1.45 ,	1.47)	1.44	(1.43 ,	1.46)	1.48	(1.47 ,	1.49)	MAT > 0°C
CNRM-ESM2-1	1.59	(1.58 ,	1.60)	1.54	(1.53 ,	1.55)	1.65	(1.64 ,	1.65)	MAT > 0°C
E3SM-1-1-ECA	1.68	(1.67 ,	1.69)	1.73	(1.72 ,	1.74)	1.58	(1.57 ,	1.59)	MAT > 0°C
IPSL-CM6A-LR	1.60	(1.58 ,	1.61)	1.54	(1.53 ,	1.56)	1.67	(1.66 ,	1.69)	MAT > 0°C
MIROC-ES2L	2.55	(2.52 ,	2.58)	2.50	(2.47 ,	2.53)	2.59	(2.56 ,	2.62)	MAT > 0°C
MRI-ESM2-0	2.98	(2.92 ,	3.03)	3.16	(3.08 ,	3.24)	2.97	(2.91 ,	3.02)	MAT > 0°C
NorESM2	1.44	(1.43 ,	1.46)	1.41	(1.40 ,	1.43)	1.47	(1.45 ,	1.48)	MAT > 0°C
CASA-CNP	2.18	(2.13 ,	2.23)	1.95	(1.91 ,	2.00)	2.29	(2.24 ,	2.34)	MAT > 0°C
MIMICS	1.44	(1.44 ,	1.45)	0.99	(0.98 ,	1.00)	1.73	(1.72 ,	1.73)	MAT > 0°C
CORPSE	1.44	(1.43 ,	1.45)	1.34	(1.33 ,	1.36)	2.07	(2.05 ,	2.08)	MAT > 0°C
Data-Product	2.25	(2.21 ,	2.30)	1.93	(1.89 ,	1.96)	2.94	(2.86 ,	3.03)	0°C < MAT < 15°C
ACCESS-ESM1-5	1.96	(1.94 ,	1.98)	1.93	(1.92 ,	1.95)	1.95	(1.93 ,	1.98)	0°C < MAT < 15°C
BCC-CSM2-MR	3.52	(3.44 ,	3.61)	2.04	(1.99 ,	2.09)	3.79	(3.70 ,	3.88)	0°C < MAT < 15°C
CESM2	2.49	(2.44 ,	2.55)	2.89	(2.82 ,	2.97)	2.15	(2.10 ,	2.21)	0°C < MAT < 15°C
CNRM-ESM2-1	1.78	(1.76 ,	1.80)	2.02	(1.99 ,	2.04)	1.58	(1.56 ,	1.60)	0°C < MAT < 15°C
E3SM-1-1-ECA	2.69	(2.64 ,	2.74)	3.00	(2.94 ,	3.06)	2.17	(2.13 ,	2.21)	0°C < MAT < 15°C
IPSL-CM6A-LR	2.04	(2.00 ,	2.08)	1.95	(1.91 ,	2.00)	2.15	(2.11 ,	2.20)	0°C < MAT < 15°C
MIROC-ES2L	3.65	(3.55 ,	3.75)	3.94	(3.83 ,	4.06)	3.51	(3.41 ,	3.60)	0°C < MAT < 15°C
MRI-ESM2-0	3.01	(2.89 ,	3.12)	2.78	(2.64 ,	2.94)	3.15	(3.03 ,	3.28)	0°C < MAT < 15°C
NorESM2	2.49	(2.42 ,	2.56)	2.84	(2.75 ,	2.93)	2.25	(2.18 ,	2.33)	0°C < MAT < 15°C
CASA-CNP	4.47	(4.21 ,	4.75)	3.76	(3.54 ,	4.00)	4.75	(4.47 ,	5.05)	0°C < MAT < 15°C
MIMICS	1.74	(1.73 ,	1.76)	1.00	(0.98 ,	1.02)	2.03	(2.01 ,	2.05)	0°C < MAT < 15°C
CORPSE	2.12	(2.09 ,	2.16)	1.90	(1.87 ,	1.93)	3.25	(3.19 ,	3.31)	0°C < MAT < 15°C
Data-Product	1.19	(1.17 ,	1.21)	1.16	(1.14 ,	1.17)	1.33	(1.30 ,	1.37)	MAT > 15°C
ACCESS-ESM1-5	2.00	(1.97 ,	2.02)	1.80	(1.78 ,	1.83)	2.10	(2.07 ,	2.14)	MAT > 15°C
BCC-CSM2-MR	1.65	(1.62 ,	1.68)	1.67	(1.64 ,	1.71)	1.66	(1.62 ,	1.69)	MAT > 15°C
CESM2	1.16	(1.14 ,	1.19)	1.05	(1.03 ,	1.07)	1.33	(1.31 ,	1.36)	MAT > 15°C
CNRM-ESM2-1	1.38	(1.36 ,	1.41)	1.21	(1.18 ,	1.23)	1.59	(1.56 ,	1.62)	MAT > 15°C
E3SM-1-1-ECA	1.18	(1.16 ,	1.21)	1.13	(1.10 ,	1.15)	1.28	(1.25 ,	1.31)	MAT > 15°C
IPSL-CM6A-LR	1.62	(1.58 ,	1.66)	1.61	(1.57 ,	1.66)	1.64	(1.60 ,	1.69)	MAT > 15°C
MIROC-ES2L	1.21	(1.17 ,	1.25)	1.08	(1.04 ,	1.12)	1.29	(1.25 ,	1.33)	MAT > 15°C
MRI-ESM2-0	2.55	(2.41 ,	2.70)	3.37	(3.12 ,	3.65)	2.41	(2.28 ,	2.55)	MAT > 15°C
NorESM2	1.17	(1.15 ,	1.20)	1.04	(1.01 ,	1.06)	1.34	(1.32 ,	1.36)	MAT > 15°C
CASA-CNP	1.35	(1.27 ,	1.44)	1.19	(1.11 ,	1.26)	1.45	(1.36 ,	1.54)	MAT > 15°C
MIMICS	1.22	(1.20 ,	1.23)	0.81	(0.79 ,	0.83)	1.57	(1.56 ,	1.58)	MAT > 15°C
CORPSE	0.84	(0.82 ,	0.86)	0.79	(0.77 ,	0.81)	1.34	(1.31 ,	1.37)	MAT > 15°C

Supplementary References:

1. Davidson, E. A. & Janssens, I. A. Temperature sensitivity of soil carbon decomposition and feedbacks to climate change. *Nature* **440**, 165–173 (2006).
2. Georgiou, K. *et al.* Global stocks and capacity of mineral-associated soil organic carbon. *Nat. Commun.* **13**, 1–12 (2022).
3. Hartley, I. P., Hill, T. C., Chadburn, S. E. & Hugelius, G. Temperature effects on carbon storage are controlled by soil stabilisation capacities. *Nat. Commun.* **12**, 1–7 (2021).
4. Manrique, L. A. & Jones, C. A. Bulk Density of Soils in Relation to Soil Physical and Chemical Properties. *Soil Sci. Soc. Am. J.* **55**, 476 (1991).
5. Alexander, E. B. Bulk Densities of California Soils in Relation to Other Soil Properties. *Soil Sci. Soc. Am. J.* **44**, 689–692 (1980).
6. Xiangsheng, Y., Guosheng, L. & Yanyu, Y. Pedotransfer Functions for Estimating Soil Bulk Density: A Case Study in the Three-River Headwater Region of Qinghai Province, China. *Pedosphere* **26**, 362–373 (2016).
7. Cotrufo, M. F., Ranalli, M. G., Haddix, M. L., Six, J. & Lugato, E. Soil carbon storage informed by particulate and mineral-associated organic matter. *Nat. Geosci.* **12**, 989–994 (2019).
8. Koven, C. D., Hugelius, G., Lawrence, D. M. & Wieder, W. R. Higher climatological temperature sensitivity of soil carbon in cold than warm climates. *Nat. Clim. Chang.* **7**, 817–822 (2017).
9. Georgiou, K. *et al.* Divergent controls of soil organic carbon between observations and process-based models. *Biogeochemistry* **2**, (2021).
10. Lawrence, C. R. *et al.* An open-source database for the synthesis of soil radiocarbon data: International Soil Radiocarbon Database (ISRaD) version 1.0. *Earth Syst. Sci. Data* **12**, 61–76 (2020).
11. Heckman, K. *et al.* Beyond bulk: Density fractions explain heterogeneity in global soil carbon abundance and persistence. *Glob. Chang. Biol.* **28**, 1178–1196 (2022).
12. Heckman, K. A. *et al.* Supporting data for manuscript: Beyond Bulk (As published in Global Change Biology) [Data set]. Zenodo (2021). doi:10.5281/zenodo.5736535
13. Shi, Z. *et al.* The age distribution of global soil carbon inferred from radiocarbon measurements. *Nat. Geosci.* **13**, 555–559 (2020).
14. Parton, W. J., Stewart, J. W. B. & Cole, C. V. Dynamics of C , N , P and S in grassland soils: a model. *Biogeochemistry* **131**, 109–131 (1988).
15. Wieder, W. R., Sulman, B. N., Hartman, M. D., Koven, C. D. & Bradford, M. A. Arctic Soil Governs Whether Climate Change Drives Global Losses or Gains in Soil Carbon. *Geophys. Res. Lett.* **46**, 14486–14495 (2019).
16. IPSL. https://forge.ipsl.jussieu.fr/orchidee/browser/branches/ORCHIDEE_3_CMIP6/ORCHIDEE/src_parameters/constantes_var.f90.
17. Parton, W. J., Del Grosso, S. J., Plante, A. F., Adair, E. C. & Lutz, S. M. *Chapter 17: Modeling the Dynamics of Soil Organic Matter and Nutrient Cycling*. *Soil Microbiology, Ecology and Biochemistry: Fourth Edition* (Elsevier Inc., 2015).
18. Parton, W. J. & Rasmussen, P. E. Long-Term Effects of Crop Management in Wheat-Fallow: II. CENTURY Model Simulations. *Soil Sci. Soc. Am. J.* **58**, 530–536 (1994).
19. Ziehn, T. *et al.* The Australian Earth System Model: ACCESS-ESM1.5. *J. South. Hemisph. Earth Syst. Sci.* **70**, 193–214 (2020).
20. Wu, T. *et al.* The Beijing Climate Center Climate System Model (BCC-CSM): The main progress from CMIP5 to CMIP6. *Geosci. Model Dev.* **12**, 1573–1600 (2019).
21. Danabasoglu, G. *et al.* The Community Earth System Model Version 2 (CESM2). *J. Adv. Model. Earth Syst.* **12**, 1–35 (2020).
22. Séférian, R. *et al.* Evaluation of CNRM Earth System Model, CNRM-ESM2-1: Role of Earth System Processes in Present-Day and Future Climate. *J. Adv. Model. Earth Syst.* **11**, 4182–4227 (2019).

23. Burrows, S. M. *et al.* The DOE E3SM v1.1 Biogeochemistry Configuration: Description and Simulated Ecosystem-Climate Responses to Historical Changes in Forcing. *J. Adv. Model. Earth Syst.* **12**, 1–59 (2020).
24. Boucher, O. *et al.* Presentation and Evaluation of the IPSL-CM6A-LR Climate Model. *J. Adv. Model. Earth Syst.* **12**, 1–52 (2020).
25. Hajima, T. *et al.* Development of the MIROC-ES2L Earth system model and the evaluation of biogeochemical processes and feedbacks. *Geosci. Model Dev.* **13**, 2197–2244 (2020).
26. Yukimoto, S. *et al.* The meteorological research institute Earth system model version 2.0, MRI-ESM2.0: Description and basic evaluation of the physical component. *J. Meteorol. Soc. Japan* **97**, 931–965 (2019).
27. Seland, Ø. *et al.* Overview of the Norwegian Earth System Model (NorESM2) and key climate response of CMIP6 DECK, historical, and scenario simulations. *Geoscientific Model Development* **13**, (2020).
28. Potter, C. S. *et al.* Terrestrial ecosystem production: A process model based on global satellite and surface data. *Global Biogeochem. Cycles* **7**, 811–841 (1993).
29. Wieder, W. R., Grandy, A. S., Kallenbach, C. M., Taylor, P. G. & Bonan, G. B. Representing life in the Earth system with soil microbial functional traits in the MIMICS model. *Geosci. Model Dev.* **8**, 1789–1808 (2015).
30. Sulman, B. N., Phillips, R. P., Oishi, a. C., Shevliakova, E. & Pacala, S. W. Microbe-driven turnover offsets mineral-mediated storage of soil carbon under elevated CO2. *Nat. Clim. Chang.* **4**, 1099–1102 (2014).
31. Wang, Y. P., Law, R. M. & Pak, B. A global model of carbon, nitrogen and phosphorus cycles for the terrestrial biosphere. *Biogeosciences* **7**, 2261–2282 (2010).
32. Randerson, T., Thompson, V., Conway, J., Fung, I. Y. & Field, B. The contribution of terrestrial sources and sinks to trends in the seasonal cycle of atmospheric carbon dioxide. *Global Biogeochem. Cycles* **11**, 535–560 (1997).
33. Cao, M. & Woodward, F. I. Net primary and ecosystem production and carbon stocks of terrestrial ecosystems and their responses to climate change. *Glob. Chang. Biol.* **4**, 185–198 (1998).
34. Lawrence, D. M. *et al.* The Community Land Model Version 5: Description of New Features, Benchmarking, and Impact of Forcing Uncertainty. *J. Adv. Model. Earth Syst.* **11**, 4245–4287 (2019).
35. Koven, C. D. *et al.* The effect of vertically resolved soil biogeochemistry and alternate soil C and N models on C dynamics of CLM4. *Biogeosciences* **10**, 7109–7131 (2013).
36. Krinner, G. *et al.* A dynamic global vegetation model for studies of the coupled atmosphere-biosphere system. *Global Biogeochem. Cycles* **19**, 1–33 (2005).
37. Ito, A. & Oikawa, T. A simulation model of the carbon cycle in land ecosystems (Sim-CYCLE): A description based on dry-matter production theory and plot-scale validation. *Ecol. Modell.* **151**, 143–176 (2002).
38. He, Y. *et al.* Radiocarbon constraints imply reduced carbon uptake by soils during the 21st century. *Science* **353**, 1419–1424 (2016).